Lamin A/C–mediated neuromuscular junction defects in Emery-Dreifuss muscular dystrophy

Alexandre Méjat,[1] Valérie Decostre,[2,3] Juan Li,[4] Laure Renou,[2] Akanchha Kesari,[5] Daniel Hantaï,[2,3] Colin L. Stewart,[6] Xiao Xiao,[4] Eric Hoffman,[5] Gisèle Bonne,[2,3,7] and Tom Misteli[1]

[1]National Cancer Institute, National Institutes of Health, Bethesda, MD 20892
[2]Institut National de la Santé et de la Recherche Médicale, Unite Mixte de Recherche U582, Institut de Myologie, Paris F-75013, France
[3]Université Pierre et Marie Curie, University Paris 06, Unite Mixte de Recherche S582, Institut Federatif de Recherche 14, Paris F-75013, France
[4]School of Pharmacy, University of North Carolina at Chapel Hill, Chapel Hill, NC 27599
[5]Research Center for Genetic Medicine, Children's National Medical Center, Washington, DC 20010
[6]Institute of Medical Biology, Immunos, Singapore City 138668, Singapore
[7]Assistance Publique, Hôpitaux de Paris, Groupe Hospitalier Pitié Salpêtrière, Unité Fonctionnelle de Cardiogénétique et Myogénétique, Service de Biochimie Métabolique, Paris F-75013, France

The *LMNA* gene encodes lamins A and C, two intermediate filament-type proteins that are important determinants of interphase nuclear architecture. Mutations in *LMNA* lead to a wide spectrum of human diseases including autosomal dominant Emery-Dreifuss muscular dystrophy (AD-EDMD), which affects skeletal and cardiac muscle. The cellular mechanisms by which mutations in *LMNA* cause disease have been elusive. Here, we demonstrate that defects in neuromuscular junctions (NMJs) are part of the disease mechanism in AD-EDMD. Two AD-EDMD mouse models show innervation defects including misexpression of electrical activity–dependent genes and altered epigenetic chromatin modifications. Synaptic nuclei are not properly recruited to the NMJ because of mislocalization of nuclear envelope components. AD-EDMD patients with *LMNA* mutations show the same cellular defects as the AD-EDMD mouse models. These results suggest that lamin A/C–mediated NMJ defects contribute to the AD-EDMD disease phenotype and provide insights into the cellular and molecular mechanisms for the muscle-specific phenotype of AD-EDMD.

Introduction

The nuclear lamina is a thin filamentous protein layer beneath the nuclear envelope made up of A- and B-type lamins, which are members of the intermediate filament family of proteins (Wilson, 2000; Burke and Stewart, 2002; Mattout et al., 2006). The *LMNA* gene encodes the A-type lamins A and C. Both proteins are important determinants of interphase nuclear architecture and play essential roles in maintaining the integrity of the nuclear envelope and chromatin structure (Mounkes et al., 2003; Burke and Stewart, 2006). Mutations in *LMNA* have been associated with a wide range of diseases, commonly referred as laminopathies (Worman and Bonne, 2007). Despite the ubiquitous expression of A-type lamins, laminopathies are highly tissue-specific and typically affect one or few selected tissues, such as adipocytes in familial partial lipodystrophy of Dunnigan type (FPLD), nerve in Charcot-Marie-Tooth disorder type 2 (CMT2B), or cardiac muscle in dilated cardiomyopathy with conduction defects (DCM-CD). Two of the most common laminopathies are Emery-Dreifuss muscular dystrophy (AD-EDMD) and limb-girdle muscular dystrophy (LGMD), which both affect skeletal and cardiac striated muscles (Broers et al., 2006). The cellular and molecular mechanisms by which mutations in genes encoding ubiquitous nuclear envelope proteins cause human disease have been largely elusive. Several possible scenarios have been suggested including impaired differentiation (Frock et al., 2006), increased susceptibility to mechanical stress (Broers et al., 2004), lamin-mediated changes in gene expression programs (Bakay et al., 2006), and alterations in lamina-associated signaling

Correspondence to Tom Misteli: mistelit@mail.nih.gov

Abbreviations used in this paper: AAV, adeno-associated virus; AChR, acetylcholine receptor; AD-EDMD, autosomal dominant Emery-Dreifuss muscular dystrophy; ALS, amyotrophic lateral sclerosis; Bgt, bungarotoxin; BMD, Becker muscular dystrophy; CMS, congenital myasthenic syndrome; CMV, cytomegalovirus; DCM-CD, dilated cardiomyopathy and conduction system disease; FPLD, Dunnigan-type familial partial lipodystrophy; *Hdac9*, histone deacetylase 9; LAP2, lamina-associated polypeptide 2; LGMD1B, limb-girdle muscular dystrophy 1B; NMJ, neuromuscular junction; shRNA, short hairpin RNA.

The Rockefeller University Press $30.00
J. Cell Biol. Vol. 184 No. 1   31–44
www.jcb.org/cgi/doi/10.1083/jcb.200811035

JCB   **31**

THE JOURNAL OF CELL BIOLOGY

events (Burke and Stewart, 2002; Mattout et al., 2006). Given the highly tissue-specific nature of laminopathies, it is possible that distinct mechanisms are responsible for defects in the various affected tissues.

The skeletal muscle tissue is composed of multinucleated fibers formed by fusion of mononucleated cells during development. Among the hundreds of nuclei in a muscle fiber, approximately four to eight nuclei are specialized for the transcription of the components of the synapse at the neuromuscular junction (NMJ; Schaeffer et al., 2001; Mejat et al., 2003). These synaptic nuclei are recruited into the vicinity of the postsynaptic membrane during muscle differentiation, and their proper positioning is crucial for NMJ establishment and maintenance (Ruegg, 2005). Positioning of synaptic nuclei at the NMJ involves the interplay between the cytoskeleton and several nuclear envelope proteins (Grady et al., 2005; Zhang et al., 2007b), including Nesprin, also known as Syne for synaptic nuclear envelope, and SUN proteins. Nesprins are a very large family of outer or inner nuclear membrane transmembrane proteins encoded by extensively alternatively spliced *SYNE1* and *SYNE2* genes (Zhang et al., 2001), which anchor nuclei to the actin cytoskeleton via a pair of calponin homology (CH) domains at the N terminus (Apel et al., 2000; Grady et al., 2005). The luminal C-terminal KASH (klarsicht/ANC-1/syne) domain of Nesprin proteins interacts with SUN proteins, which span the inner nuclear membrane and physically interact with A-type lamins, establishing a continuous physical link between the nuclear lamina and the cytoskeleton (Starr and Han, 2002; Padmakumar et al., 2005; Crisp et al., 2006; Haque et al., 2006). Double knockout of Nesprin-1 and Nesprin-2 in mice leads to the complete absence of nuclei recruited to the synapses of diaphragm muscles (Zhang et al., 2007b), which demonstrates the importance of nuclear envelope components in synaptic nuclei positioning.

We hypothesized that A-type lamins might contribute to the proper positioning of synaptic nuclei at the NMJ in muscle fibers, and, hence, we sought to test the possibility that A-type lamins–mediated NMJ defects contribute to AD-EDMD disease symptoms. Here, we show that $Lmna^{H222P/H222P}$ and $Lmna^{-/-}$ mice, two previously described AD-EDMD mouse models, fail to innervate muscle and exhibit aberrant NMJ architecture. In both mice models, several nuclear envelope components crucial for proper recruitment and positioning of synaptic nuclei are mislocalized, leading to a reduction in their number and their mispositioning at the NMJ. Consequently, $Lmna^{H222P/H222P}$ and $Lmna^{-/-}$ muscles show misexpression of electrical activity–dependent genes and altered epigenetic chromatin modifications. The same defects were present in biopsies from AD-EDMD patients, which indicates that these defects are relevant to human disease. The sum of our results suggests that failed muscle innervation contributes to AD-EDMD.

Results

Muscle innervation defects in AD-EDMD mouse models

To test whether AD-EDMD pathology involves muscle–nerve interaction defects, we analyzed innervation patterns in $Lmna^{-/-}$

and $Lmna^{H222P/H222P}$ mice. Mice lacking the $Lmna$ gene die 6–7 wk after birth because of severe muscular dystrophy and cardiomyopathy, resembling AD-EDMD (Sullivan et al., 1999), and present an axonopathy (De Sandre-Giovannoli et al., 2002). $Lmna^{H222P/H222P}$ mice carry a missense mutation that was originally identified in a family with AD-EDMD (Arimura et al., 2005). Adult H222P homozygous male mice exhibit several symptoms reminiscent of AD-EDMD patients including reduced locomotion with abnormal stiff walking posture, cardiac fibrosis, chamber dilatation, and hypokinesia with conduction defects, and they typically die by 9 mo of age (Arimura et al., 2005).

When compared with wild-type littermates of identical genetic background, we found innervation defects in both animal models in the diaphragm visualized by staining for bungarotoxin (Bgt), which specifically binds to the acetylcholine receptors (AChR) accumulated at the muscle motor synapses (Fig. 1, A, C, and E). In wild-type animals, synapses are concentrated in a narrow band, and AChR clusters appear as a thin line in the middle of each hemidiaphragm muscle (Fig. 1 A). In contrast, in diaphragms of $Lmna^{H222P/H222P}$ and $Lmna^{-/-}$ animals, neuromuscular synapses are present outside of the central narrow end-plate band region, and synapses are scattered over a wider area of the muscle (Fig. 1, C and E). Quantitative analysis demonstrated that although the innervation area is limited to an $\sim$1-mm-wide band in wild-type animals (990 ± 281 µm and 1,027 ± 283 µm at 6 wk and 6 mo, respectively), it extends by an additional 40% in adult $Lmna^{H222P/H222P}$ (1,387 ± 418 µm; P < 0.001) and by 70% in the phenotypically more severely affected 6-wk-old $Lmna^{-/-}$ mice (1,775 ± 580 µm; P < 0.001; Fig. 1 I). In addition to the size of the postsynaptic innervation area, the branching pattern of the diaphragm's motor nerve was also affected in AD-EDMD mouse models (Fig. 1, B, D, and F). In contrast to wild-type animals where phrenic nerves, visualized by double-staining for neurofilament 150 kD and synaptophysin, showed few ramifications, phrenic nerves in $Lmna^{H222P/H222P}$ and $Lmna^{-/-}$ animals were highly branched and extended to a large area from the center of the diaphragm, with some ramifications covering the whole surface of the diaphragm (Fig. 1 B, D, and F, arrowhead). Compared with the wild type, $Lmna^{-/-}$ diaphragms showed intense nerve sprouting from both the main nerve axis and secondary branches (Fig. 1, G and H). The substantially altered innervation pattern pointed to a failure of motor nerves to innervate muscle fibers in $Lmna^{-/-}$ and $Lmna^{H222P/H222P}$ muscle fibers.

Abnormal NMJ morphology in AD-EDMD mouse models

To assess whether the structure of individual muscle synapses was affected in AD-EDMD mouse models, we compared the NMJ morphology in isolated fibers from wild-type, $Lmna^{H222P/H222P}$, and $Lmna^{-/-}$ tibialis anterior muscles using Bgt staining (Fig. 2). In NMJs from wild-type muscle, AChR clusters form a typical continuous branched network (Fig. 2 A). Compared with wild-type animals, $Lmna^{H222P/H222P}$ and $Lmna^{-/-}$ synapses were markedly altered. The AChR network was usually discontinuous in $Lmna^{H222P/H222P}$ muscle, and several independent AChR clusters were frequently observed, which suggests a fragmentation of the
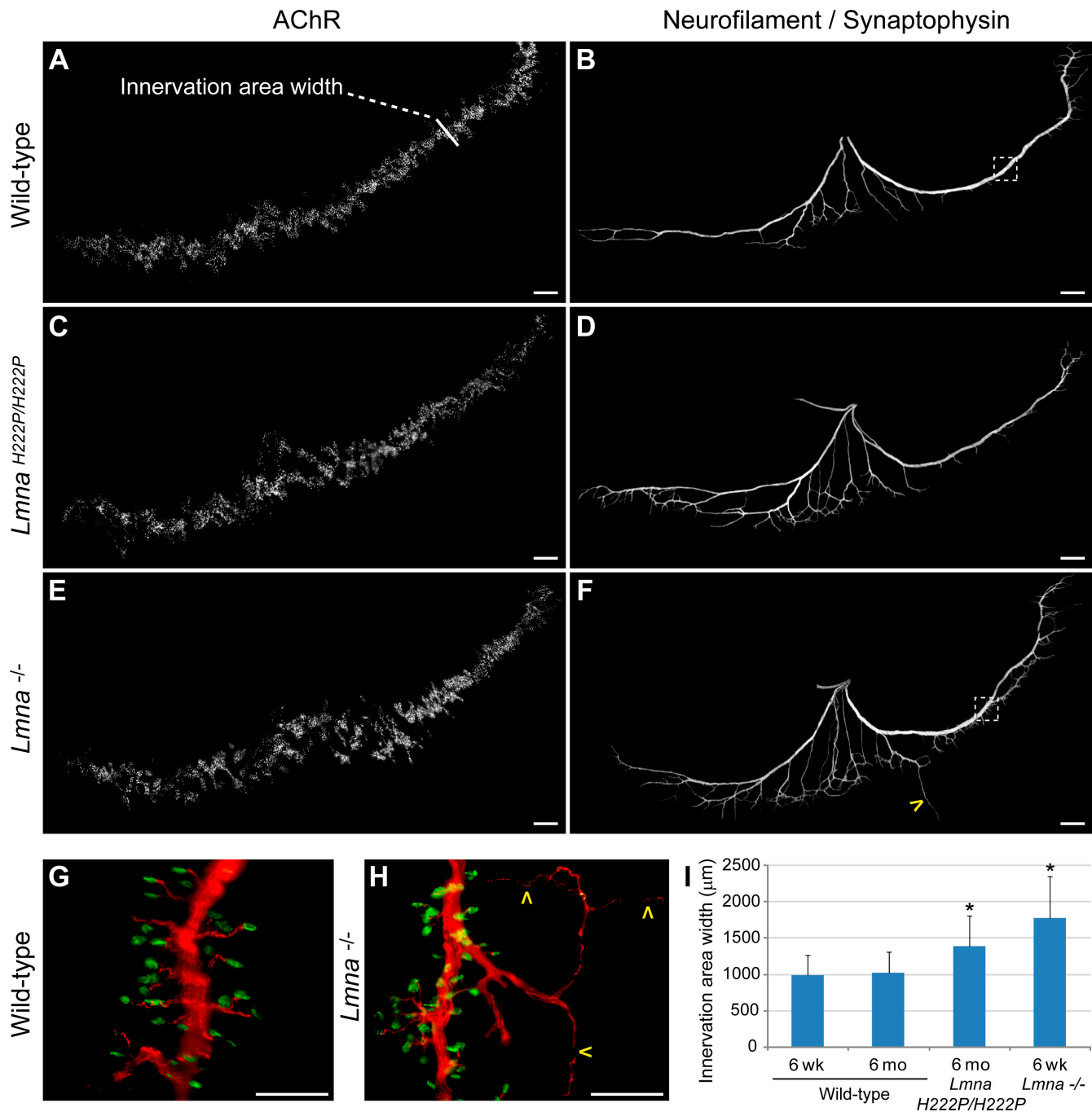
Figure 1. **Innervation patterns in wild-type and AD-EDMD mouse models.** Whole-mount diaphragms of 6-mo-old wild-type (A and B), 6-mo-old *Lmna^H222P/H222P* (C and D), and 6-wk-old *Lmna^−/−* (E and F) mice were stained with Bgt to delineate the NMJs (AChR; A, C, and E), and neurofilament p150 and synaptophysin were used to stain the motor axon (B, D, and F). A representative right hemidiaphragm of each phenotype is shown. *Lmna^H222P/H222P* and *Lmna^−/−* diaphragms showed markedly broader synapse bands (A, C, and E) and highly ramified phrenic nerves (B, D, and F). (G and H) Enlargements of indicated areas (boxes in B and F) double-stained with neurofilament/synaptophysin (red) and Bgt (green) showing intense nerve sprouting from both the main nerve axis and secondary branches in *Lmna^−/−* diaphragm (arrowheads). (I) Quantitation of postsynaptic innervation area width. Values shown are mean ± SD of at least 200 measurements per diaphragm from three mice per genotype. *, P < 0.001 relative to wild-type littermate mice. Bars, 500 μm.

NMJ (Fig. 2 B). Even more pronounced defects were present in muscle from *Lmna^−/−* animals, where AChR networks were often dramatically disorganized, with fewer discernable individual branches and aggregated AChR clusters (Fig. 2 C). These observations were confirmed by quantitative analysis based on Bgt staining and AChR organization (Fig. 2 D). About 86.7 ± 4.3% of synapses showed altered morphology in 6-wk-old *Lmna^−/−* mice,

and 72.3 ± 2.6% of synapses were abnormal in 6-mo-old *Lmna^H222P/H222P* mice, which showed slightly milder symptoms (Arimura et al., 2005). Importantly, a significant fraction of ∼50% of NMJs was already abnormal in 6-wk-old *Lmna^H222P/H222P* mice, which do not yet show apparent muscle and locomotion defects. These data point to the possibility that NMJ disorganization takes place before the overt myopathic phenotype.
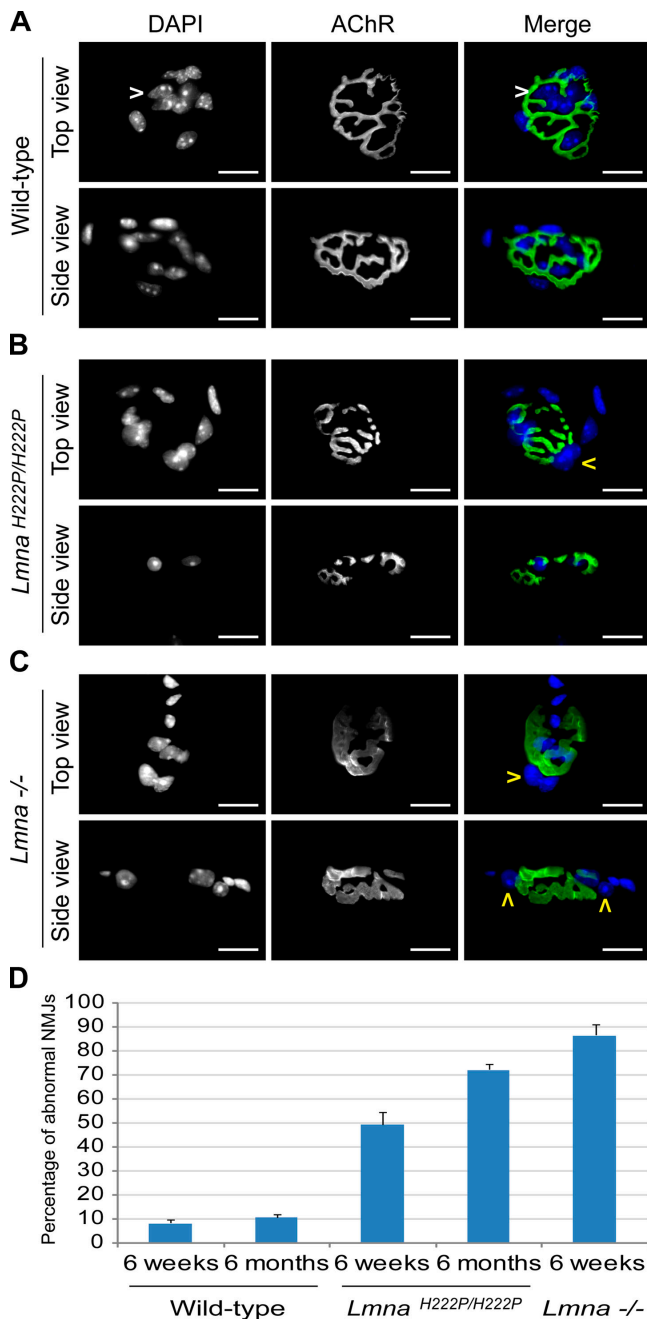
Figure 2. **Abnormal NMJs in muscle from wild-type and AD-EDMD mouse models.** (A–C) Representative synapse morphologies from wild-type, $Lmna^{H222P/H222P}$, and $Lmna^{-/-}$ mice isolated fibers from tibialis anterior stained with DAPI and Bgt. (A) Synapses from 6-mo-old wild-type mice showed characteristic "pretzel-like" AChR networks, and between four and eight nuclei directly aggregated beneath the NMJ (white arrowheads). (B) Synapses from 6-mo-old $Lmna^{H222P/H222P}$ were frequently fragmented with muscle nuclei located at the periphery of the AChR network (yellow arrowhead). (C) AChR staining in 6-wk-old $Lmna^{-/-}$ muscles was generally dramatically disorganized, with barely discernable branches, whereas few to no nuclei were observed underneath or at the periphery (yellow arrowheads) of the NMJ. (D) The percentage of abnormal NMJs observed in 6-wk-old and 6-mo-old wild-type, $Lmna^{H222P/H222P}$, and $Lmna^{-/-}$ mice muscles. Values are mean ± SD of at least 100 NMJ from three different animals in each genotype. Bars, 10 µm.

Mislocalization of nuclear positioning components in AD-EDMD mouse muscle

To address the molecular mechanism by which $Lmna$ mutations lead to altered NMJ morphology, we probed the localization of several prominent lamin A/C–interacting proteins in synaptic nuclei. Lamin B1, all isoforms of the lamina-associated polypeptide 2 (LAP2), and SUN1 proteins were unaffected in $Lmna^{-/-}$ and $Lmna^{H222P/H222P}$ muscle (not depicted and Fig. S1 A, available at http://www.jcb.org/cgi/content/full/jcb.200811035/DC1). However, the distribution of the inner nuclear membrane protein SUN2 was dramatically altered in synaptic nuclei of $Lmna^{-/-}$ and $Lmna^{H222P/H222P}$ muscle (Fig. 3 A). Although the protein was evenly distributed and enriched in the nuclear envelope in synaptic nuclei of wild-type animals (Figs. 3 A and S1 A), SUN2 was frequently aggregated on one side of synaptic nuclei in $Lmna^{-/-}$ and $Lmna^{H222P/H222P}$ muscle (Fig. 3 A). Aberrant SUN2 staining was specific for synaptic nuclei, as its localization pattern was generally indistinguishable in extrasynaptic nuclei from the wild type and both mouse models (Fig. S1 B). Occasionally, SUN2 was found punctuated in extrasynaptic nuclei, but only in $Lmna^{-/-}$ highly atrophic fibers (Fig. S1 C).

Muscle nuclei from $Lmna^{-/-}$ and $Lmna^{H222P/H222P}$ mice also exhibited pronounced mislocalization of the outer nuclear envelope protein Nesprin-1 (Fig. 3 B). As previously reported, in wild-type muscle fibers, Nesprin-1 was expressed in all muscle nuclei and highly enriched at the synaptic nuclear envelope but was hardly detectable in Schwann cell nuclei (Fig. 3 B; Apel et al., 2000). Although Nesprin-1 localization and intensity was not altered in extrasynaptic nuclei of $Lmna^{-/-}$ and $Lmna^{H222P/H222P}$ muscle fibers (Fig. S1 B), perinuclear Nesprin-1 staining was reduced in $Lmna^{H222P/H222P}$ and $Lmna^{-/-}$ synaptic nuclei compared with wild-type animals (Fig. 3 B). Collectively, these observations demonstrate that the absence of A-type lamins or H222P mutation affects synaptic nuclear envelope organization but has little effect on localization of Nesprin-1 in extrasynaptic nuclei, which supports a role of A-type lamins in NMJ formation or maintenance.

Muscle from AD-EDMD mouse models fails to recruit synaptic nuclei

SUN and Nesprin have been implicated in positioning nuclei via their interaction with A-type lamins (Haque et al., 2006; Worman and Gundersen, 2006). Given the aberrant localization of SUN2 and Nesprin-1, we tested whether the localization of nuclei to the NMJ was affected in AD-EDMD mouse models. Normal NMJs are characterized by tight clustering of several muscle nuclei directly underneath the postsynaptic membrane (Fig. 4 A). Compared with NMJs in wild-type animals, $Lmna^{H222P/H222P}$ and $Lmna^{-/-}$ synapses showed less muscle nuclei, most of them being located at the immediate synapse periphery in a pattern similar to that of aberrantly localized nuclei in dominant-negative Nesprin-1 transgenic mice (Fig. 4 A; Grady et al., 2005). Quantitation of the number of synaptic and perisynaptic nuclei defined by Nesprin-1 staining (Fig. 4 A; Grady et al., 2005) demonstrated that although in 6-wk-old wild-type muscle, 4.5 ± 0.76 muscle nuclei are found aggregated beneath the AChR clusters and almost no nuclei were found in a perisynaptic position (Fig. 4 B and C),
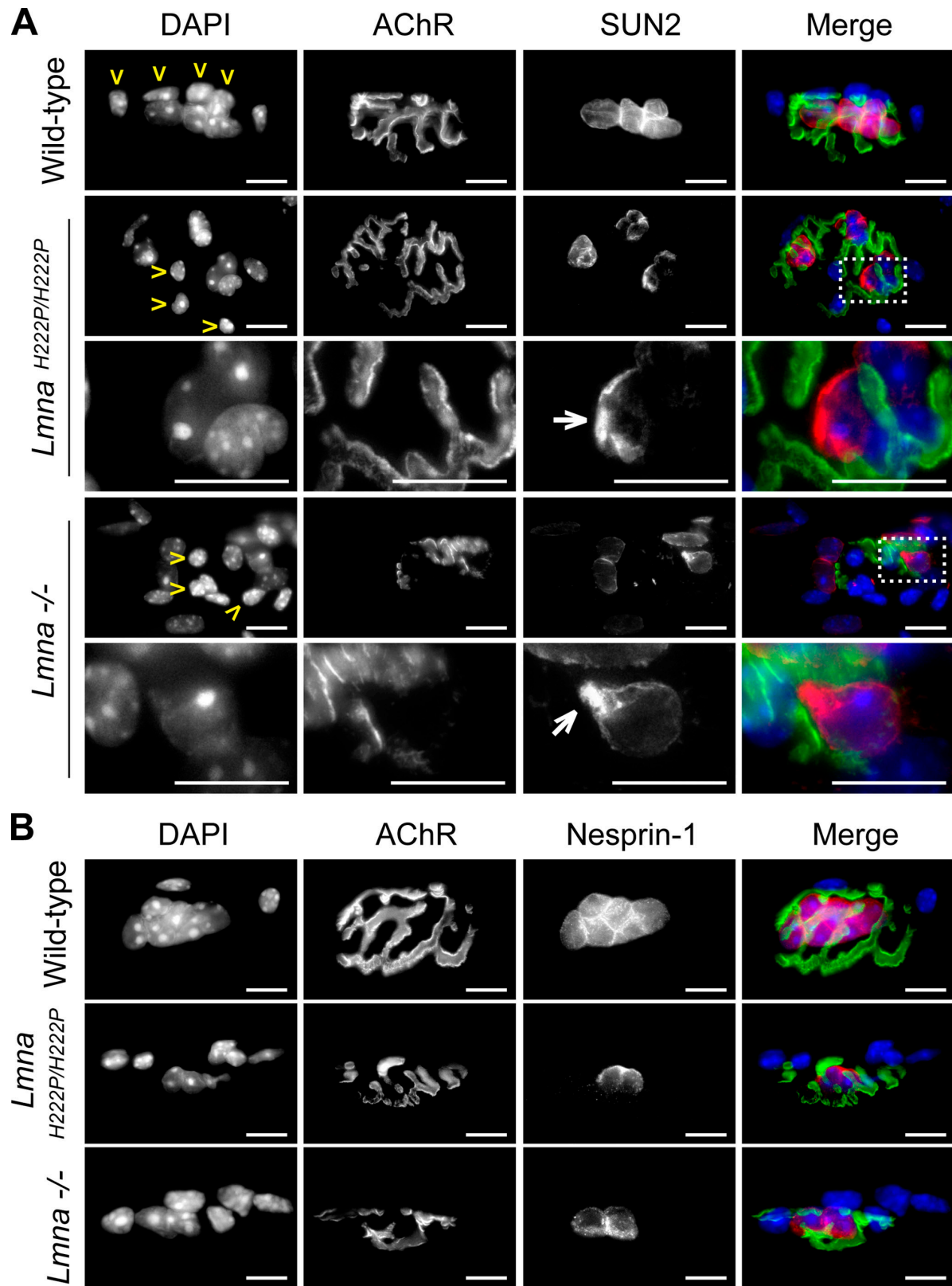
Figure 3. **Mislocalization of nuclear envelope components in synaptic nuclei of AD-EDMD mouse models.** Isolated muscle fibers from 6-mo-old wild-type, 6-mo-old *Lmna*[H222P/H222P], and 6-wk-old *Lmna*^{−/−} mice tibialis anterior muscles were stained with DAPI, Bgt, and SUN2 (A) or Nesprin-1 antibodies (B). SUN2 and Nesprin-1 were expressed in all muscle nuclei but with a lower staining in mutant synaptic nuclei (A and B). Boxes indicate the area enlarged in the panel below. Compared with wild type, SUN2 appeared heterogeneous and frequently aggregated on one side of synaptic nuclei in AD-EDMD mouse models (A, white arrows). Nesprin-1 staining was reduced in *Lmna*[H222P/H222P] and *Lmna*^{−/−} synaptic nuclei and partly relocalized (B). In all cases, Schwann cell nuclei (yellow arrowheads) were negative for both Nesprin-1 and SUN2. Bars, 10 μm.
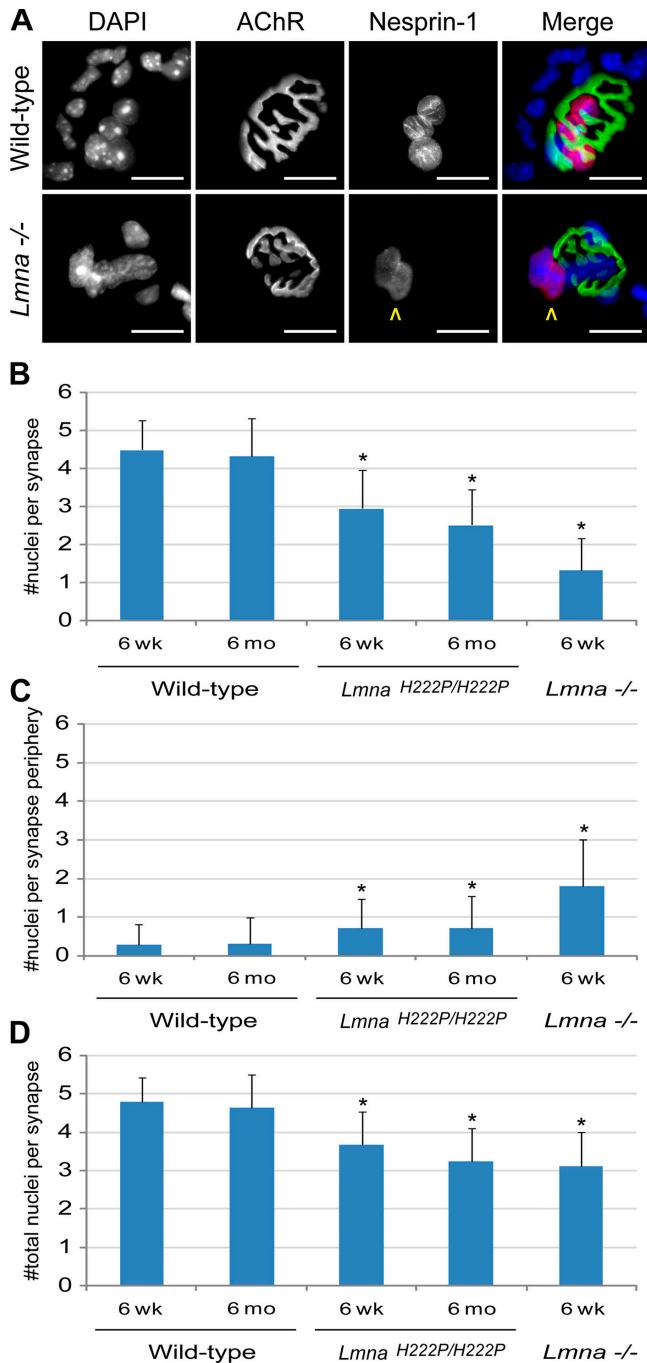
Figure 4. Altered recruitment of the muscle synaptic nuclei. (A) Isolated muscle fibers were stained with DAPI, Bgt, and Nesprin-1 antibodies to unequivocally identify synaptic myonuclei (yellow arrowheads). Bars, 10 µm. (B–D) Nesprin-1–positive myonuclei were quantified according to their relative position to the Bgt staining. Percentage of synaptic (B), perisynaptic (C), and total (D) nuclei per muscle synapse of 6-wk-old and 6-mo-old wild-type, 6-wk-old and 6-mo-old $Lmna^{H222P/H222P}$, and 6-wk-old $Lmna^{-/-}$ mice are shown. Values are mean ± SD of at least 100 NMJs from three different animals in each genotype. *, P < 0.001 relative to littermate wild type.

in age-matched $Lmna^{-/-}$ synapses, only 1.3 ± 0.8 nuclei were at the synapse, and typically, approximately two nuclei were found in a perisynaptic position. Consistent with these observations, quantification of total nuclei per synapse (Fig. 4 D) showed a global decrease in the number of muscle nuclei recruited to

$Lmna^{-/-}$ synapses (3.1 ± 0.9 nuclei per synapse) compared with wild-type synapses (4.8 ± 0.6 nuclei per synapse), which suggests that in the absence of functional A-type lamins, both positioning and recruitment of synaptic nuclei are affected.

In line with their milder muscular phenotype, synapses from 6-mo-old $Lmna^{H222P/H222P}$ showed a significant, albeit less dramatic, reduction in the number of muscle nuclei recruited to the synapse sites (2.5 ± 0.9 synaptic nuclei per synapse and 3.2 ± 0.9 total nuclei per synapse) compared with 6-mo-old wild-type muscles (4.3 ± 1.0 synaptic nuclei per synapse and 4.6 ± 0.9 total nuclei per synapse). Interestingly, at 6 wk, when $Lmna^{H222P/H222P}$ animals are still asymptomatic, synapses already had a reduced number of nuclei (2.9 ± 1.0 synaptic nuclei; 3.7 ± 0.9 total nuclei per synapse) compared with wild-type littermate animals, which further supports the notion that NMJ defects occur before muscle symptoms (Fig. 4, B–D). From these observations, we concluded that the absence of A-type lamins or some $Lmna$ mutations contribute to failed recruitment and positioning of nuclei at the NMJ in AD-EDMD mouse models.

Functional consequences of NMJ defects in AD-EDMD mouse models

To assess the functional consequences of morphological NMJ defects in $Lmna^{H222P/H222P}$ and $Lmna^{-/-}$ mice, we probed gene expression levels of several electrical activity–dependent genes by quantitative RT-PCR in wild-type, $Lmna^{H222P/H222P}$, and $Lmna^{-/-}$ muscle (Fig. 5 A). AChR-γ subunit ($Chrng$) expression is normally restricted to embryonic development and is repressed by muscle innervation (Schaeffer et al., 2001; Mejat et al., 2003), but pathological inefficient neurotransmission or experimental denervation leads to reexpression of $Chrng$ in adult muscle fibers (Chevessier et al., 2004; Mejat et al., 2005). Similarly, $Chrng$ levels were significantly up-regulated by 8- and 14-fold in muscle from 6-mo-old $Lmna^{H222P/H222P}$ and 6-wk-old $Lmna^{-/-}$ mice, respectively, compared with wild-type muscle (Fig. 5 A). Likewise, muscle innervation normally represses expression of the AChR-α subunit ($Chrna$) in extrasynaptic myonuclei, restricting its expression to synaptic nuclei (Schaeffer et al., 2001; Mejat et al., 2003). In inefficient neurotransmission and experimental denervation, nonsynaptic nuclei reexpress $Chrna$ (Duclert et al., 1991; Merlie et al., 1994). Similar to denervated muscle, $Lmna^{-/-}$ and $Lmna^{H222P/H222P}$ muscle overexpressed $Chrna$ 2.7- and 2.2-fold compared with littermate wild-type muscle (Fig. 5 A). Furthermore, the myogenic regulatory factors MyoD ($Myod1$) and myogenin ($Myog$), which are down-regulated in adult innervated muscle fiber and reexpressed in inefficient neurotransmission and upon experimental denervation (Merlie et al., 1994), were up-regulated between 2.5- and 6.1-fold in $Lmna^{H222P/H222P}$ and $Lmna^{-/-}$ muscles (Fig. 5 A). Histone deacetylase 9 ($Hdac9$), which controls $Myod1$ and $Myog$ in an electrical activity–dependent fashion (Mejat et al., 2005), was down-regulated twofold in $Lmna^{-/-}$ and $Lmna^{H222P/H222P}$ muscle, similar to what is observed in experimentally denervated muscle (Mejat et al., 2005). Finally, as in denervated muscle, atrogin-1 ($Fbxo32$), a strong marker of denervation-induced muscle atrophy (Gomes et al., 2001; Sandri et al., 2004), was overexpressed 2.7- and 2.9-fold in
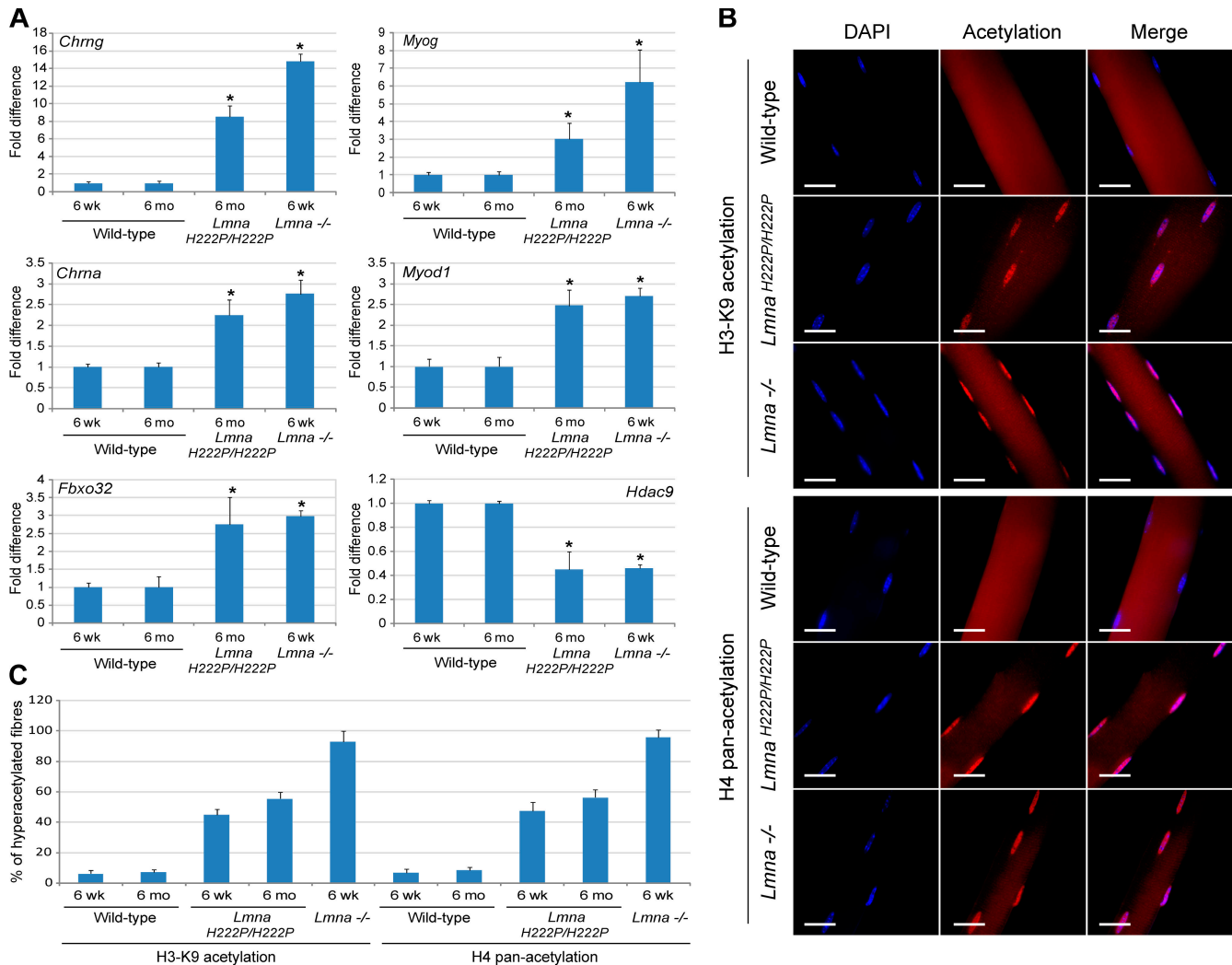
Figure 5. **Hallmarks of denervation in AD-EDMD mouse models.** (A) mRNA expression levels of *Chrng*, *Chrna*, *Myog*, *MyoD1*, *Fbxo32*, and *Hdac9* were evaluated in wild-type, *Lmna*^{H222P/H222P}, and *Lmna*^{−/−} mice gastrocnemius muscles by quantitative RT-PCR (A). Mutant muscles showed higher expression levels of electrical activity–dependent genes (*Chrng*, *Chrna*, *Myog*, and *MyoD1*) and atrophy-associated genes (*Fbxo32*). In contrast, mutant muscles expressed less *Hdac9* than the wild type. All gene expression levels were normalized to *Gapdh*. Values are mean ± SD from six muscles (two muscles from three mice) per genotype. *, P < 0.001 relative to the wild type. Expression levels in each sample were evaluated in at least two independent quantitative RT-PCR experiments. (B) Wild-type and *Lmna* mutant isolated muscle fibers from tibialis anterior muscle were stained with DAPI, Bgt, and acetylated histone H3-K9 or acetylated histone H4 antibodies. A high proportion of *Lmna*^{H222P/H222P} and *Lmna*^{−/−} fibers displayed increased histone acetylation levels. The percentage of histone hyperacetylated muscle fibers are indicated for the different genotypes. Values are means ± SD from at least 100 fibers from three different mice per genotype. Bars, 25 µm.

Lmna^{−/−} and *Lmna*^{H222P/H222P} muscle, respectively (Fig. 5 A). As a control, the levels of AChR-ε subunit (*Chrne*), which is known to be independent of electrical activity (Duclert et al., 1991), were unchanged in *Lmna*^{−/−} and *Lmna*^{H222P/H222P} muscle (not depicted). We conclude that *Lmna*^{−/−} and *Lmna*^{H222P/H222P} muscle gene expression patterns are highly similar to those observed in denervated muscle.

A further hallmark of denervated muscle is an increase in histone acetylation, likely as a consequence of *Hdac9* down-regulation (Mejat et al., 2005). To assess whether global chromatin modifications are also present in the two animal models, we stained isolated wild-type, *Lmna*^{−/−}, and *Lmna*^{H222P/H222P} muscle fibers using antibodies against acetylated histone H3 lysine 9 (H3-AcK9) or pan-acetylated histone H4 (panAc-H4). As described previously (Ravel-Chapuis et al., 2007), we observed ele-

vated H3-K9 and pan-H4 acetylation in synaptic nuclei compared with extrasynaptic nuclei in wild-type muscle fibers (Fig. S2, available at http://www.jcb.org/cgi/content/full/jcb.200811035/DC1). However, compared with wild-type muscle, histones H3-K9 and H4 acetylation levels were strongly increased in *Lmna*^{−/−} and *Lmna*^{H222P/H222P} muscle extrasynaptic nuclei (Fig. 5 B) and were comparable in synaptic nuclei (Fig. S2). To verify that this extrasynaptic nuclei histone hyperacetylation was related to a defect in neuromuscular transmission, we quantified the number of hyperacetylated fibers in each type of mutant muscle (Fig. 5 B). We found that the percentage of hyperacetylated fibers accompanies muscle defects (Fig. 5 C). More than 90% of fibers were globally hyperacetylated in the severely affected *Lmna*^{−/−} mice, ∼70% were hyperacetylated in the more mildly affected 6-mo-old *Lmna*^{H222P/H222P} mice, and 40% were hyperacetylated in the
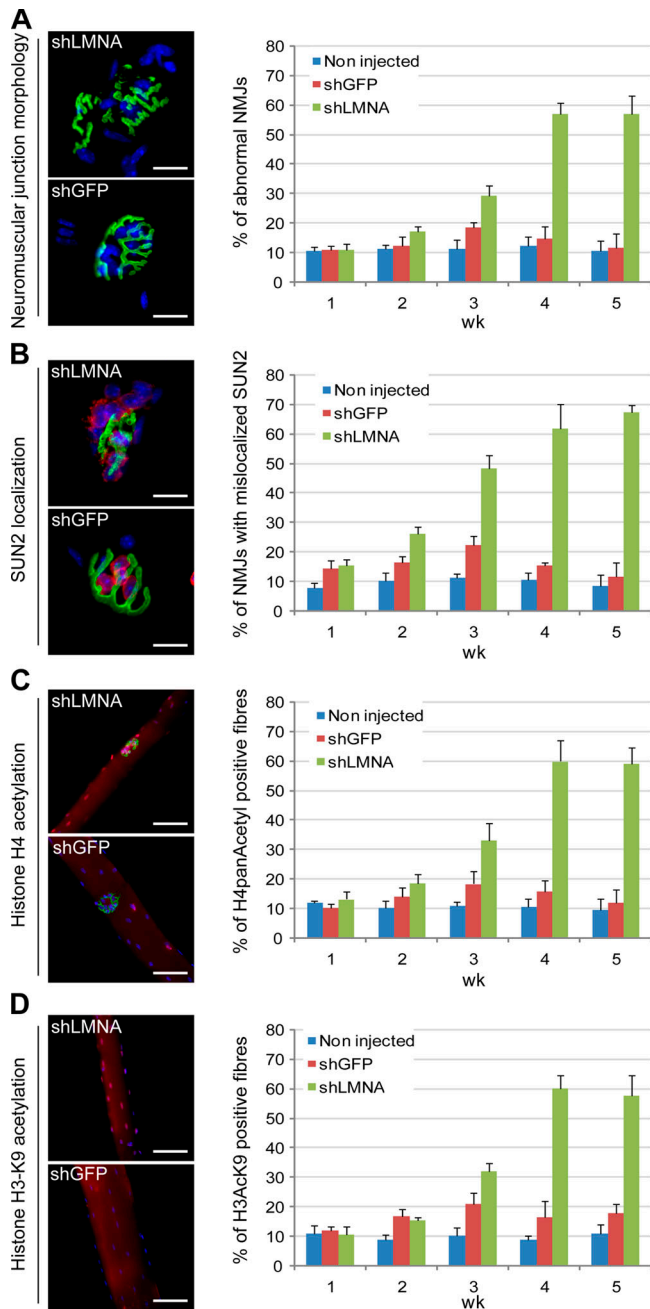
Figure 6. **Transient A-type lamin knockdown in wild-type tibialis anterior.** Wild-type tibialis anterior muscles injected with AAV6 expressing shRNAs against *LMNA* (shLMNA) or GFP (shGFP) were assessed at the indicated time after AAV injection for several phenotypes observed in *Lmna*[H222P/H222P] and *Lmna*^{−/−} muscles: NMJ morphology (A), SUN2 localization (B), and H3 and H4 histone acetylation levels (C and D). For each assay, a representative NMJ or muscle fiber from shLMNA- or shGFP-injected muscle 4 wk after injection is provided with the quantification of the number of altered NMJ per fiber at each time point. Hyperacetylated nuclei visible on shGFP (C) correspond to nuclei from nonmuscle interstitial cells and were used as positive controls for the staining. Values are means ± SD from at least 100 fibers from three different mice per criteria.

asymptomatic 6-wk-old *Lmna*[H222P/H222P] mice, compared with ∼7% in wild-type mice (Fig. 5 C). These numbers are also similar to the percentage of abnormal NMJs in the three groups of AD-EDMD mice (Fig. 2).

Transient A-type lamin knockdown in wild-type tibialis anterior recapitulates NMJ defects

To confirm that the observed NMJ defects were a direct cause of A-type lamins loss and not caused by an indirect nerve defect, we knocked down A-type lamins in tibialis anterior muscle of wild-type animals using adeno-associated viruses (AAV) expressing short hairpin RNAs (shRNAs) against LMNA. In pilot experiments to optimize viral transduction, injection of AAV6–GFP virus into muscle resulted in expression of the GFP transgene in >90% of muscle cells 1 wk after transduction; expression was limited to muscle and was absent from Schwann cells and neurons (Fig. S3 A, available at http://www.jcb.org/cgi/content/full/jcb.200811035/DC1). Injection of AAV6 expressing shRNA against A-type lamins (AAV6-shLMNA) in tibialis anterior muscle, but presumably not in adjacent neurons, resulted in an ∼70% decrease of A-type lamin protein levels 2 wk after injection, and was maintained 5 wk after injection (Fig. S3 B). No decrease in A-type lamin mRNA or protein levels occurred in the noninjected tibialis interior control muscle over the same time period in the same animal injected with AAV6 expressing shRNA against GFP (AAV6-shGFP; Fig. S3 B).

Knockdown of A-type lamins in muscle from wild-type animals recapitulated the NMJ defects observed in AD-EDMD mouse models. After 3 wk, we observed a significant increase in the number of fragmented NMJs in tibialis anterior muscles injected with AAV6-shLMNA, whereas AAV6-shGFP–injected control muscles only showed a slight variation compared with noninjected muscle (Fig. 6 A). 4 and 5 wk after injection, ∼60% of the NMJs showed an altered morphology in AAV6-shLMNA–injected muscle, whereas in AAV6-shGFP and in noninjected control muscle, only 10–15% of NMJs were abnormal (Fig. 6 A). Similarly, as in the AD-EDMD mouse models, SUN2 proteins were frequently mislocalized and aggregated in synaptic nuclei of tibialis anterior muscle injected with AAV6-shLMNA, whereas SUN2 staining was homogeneous and indistinguishable from wild-type animals in AAV6-shGFP–injected muscles (Fig. 6 B). Interestingly, SUN2 localization was frequently found altered in NMJs, which still showed normal AChR organization, suggesting that SUN2 reorganization precedes NMJ architecture defects (Fig. 6 B). As observed in the AD-EDMD mouse models, SUN2 staining was not affected in extrasynaptic nuclei of AAV6-shLMNA–injected muscles (not depicted). Finally, the number of hyperacetylated muscle fibers (histones H4 and H3-K9) strictly correlated with the proportion of abnormal NMJs in injected tibialis anterior muscles and reached ∼60% in AAV6-shLMNA–injected tibialis anterior muscles 4 wk after injection, but was only slightly higher in AAV6-shGFP–injected muscles than in noninjected muscle (Fig. 6, C and D). Collectively, these results demonstrate that the observed NMJ defects are directly mediated by A-type lamins and that their loss in the muscle, but not in the nerve itself, is sufficient to cause AD-EDMD symptoms.

Denervation hallmarks in AD-EDMD patients

To finally assess whether the NMJ defects we observed in AD-EDMD mouse models also occurred in human AD-EDMD
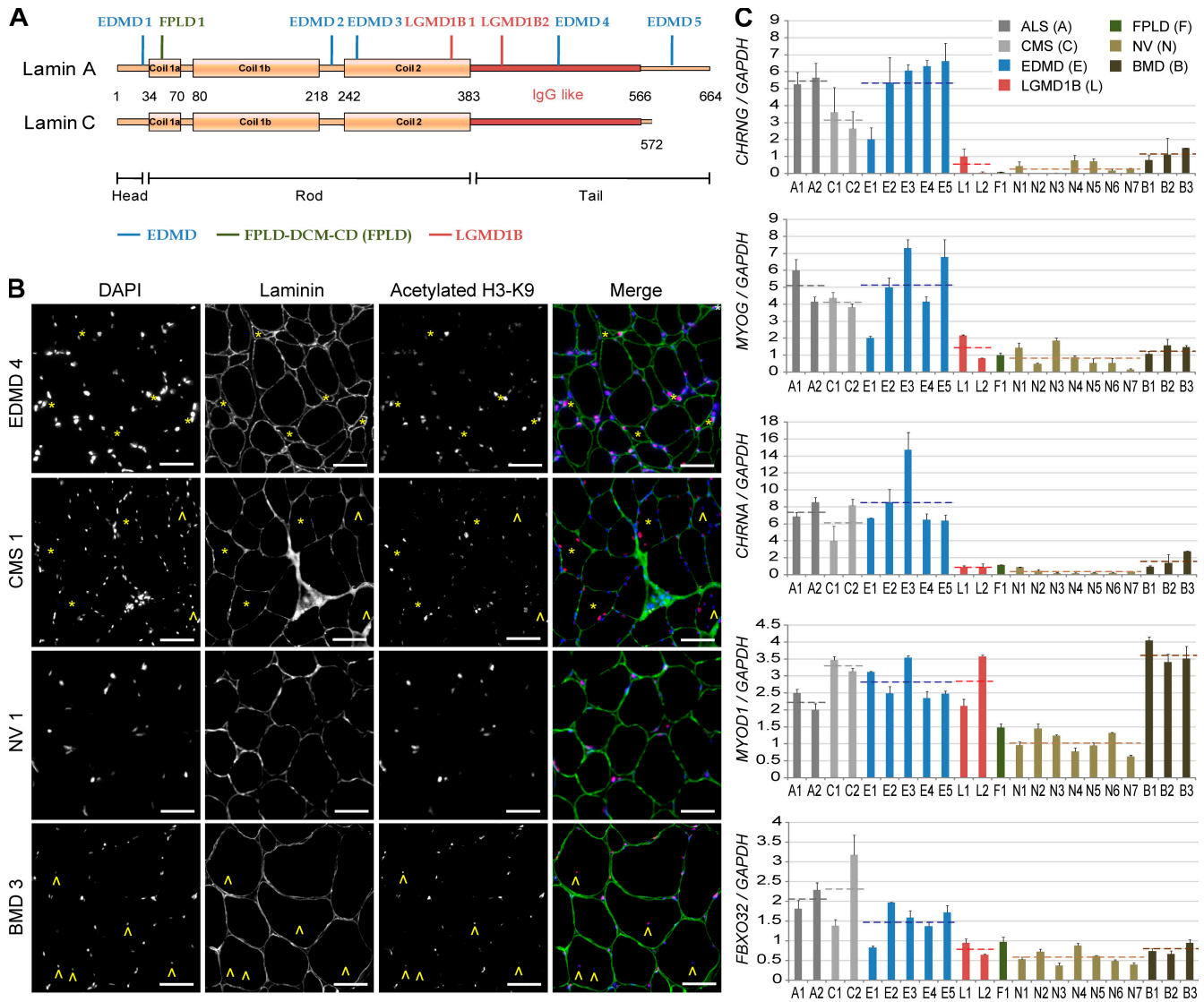
Figure 7. **Hallmarks of denervation in human patients.** (A) Schematic representation of A-type lamin proteins. The position of the different mutations studied is indicated along the length of the protein. (B) Muscle biopsies from AD-EDMD, BMD, and CMS patients as well as normal volunteer (NV) were stained with DAPI (blue), α2-laminin antibody (green), and acetylated-histone H3-lysine 9 (K9) antibody (red). Atrophic muscle fibers (asterisks) showed a very high level of acetylation and no grouping of atrophic fibers. Muscle fibers of normal size occasionally showed hyperacetylated nuclei in AD-EDMD muscles. In contrast, hyperacetylated nuclei were only observed in nonmuscle interstitial cells in NV muscles. Although many centrally located nuclei could be observed in BMD muscles (arrowheads), most nuclei were in a subsarcolemmal position in AD-EDMD and CMS patients and in NV muscles. Bars, 30 µm. (C) Expression levels of *CHRNG, CHRNA, MYOG, MYOD1,* and FBXO32 were evaluated by quantitative RT-PCR on human biopsies. Patients affected by AD-EDMD were compared with patients affected by LGMD1B, FLPD-DCM-CD, ALS, CMS, BMD, and NV. Compared with NV, EDMD patients showed high, though similar to denervation-related diseases (ALS and CMS), levels of *CHRNG, CHRNA, MYOG,* and *FBXO32.* In contrast, expression levels of patients affected by the nondenervation-related disease BMD were similar to NV. Patients affected by other laminopathies (LGMD1B and FPLD-DCM-CD) showed low, though similar to normal volunteers, levels of *CHRNG, CHRNA,* and *MYOG.* All patients affected by neuromuscular diseases (ALS, CMS, EDMD, LGMD1B, and BMD) showed a high level of *MYOD1* compared with NV but this could be caused by two independent mechanisms: misregulation in the muscle fibers (ALS, CMS, and potentially EDMD) and/or regeneration by the activated satellite cells (BMD). All gene expression levels were normalized to the *GAPDH* expression level. Values provided for each patient are means ± SD from at least three independent experiments. Broken lines indicate mean values of a group of patients.

patients, histological features, gene expression of denervation markers, and global histone acetylation were evaluated in human muscles biopsies. Morphological innervation and NMJ defects cannot be assessed in human samples because of the scarcity of NMJs in muscle biopsies. Histology and expression of the electrical activity–dependent genes *CHRNG, CHRNA,* and *MYOG* and the muscle atrophy gene *FBXO32* were evaluated in five AD-EDMD patient biopsies representing five different characterized mutations in *LMNA* affecting different domains in the protein (Fig. 7 A and Table S1, available at http://www.jcb.org/cgi/content/full/jcb.200811035/DC1); these were compared with normal volunteer biopsies (Table S1). As further controls, we used patients affected by the established denervation syndrome amyotrophic lateral sclerosis (ALS) and the NMJ disease congenital myasthenic syndrome (CMS); and as a negative control, we used biopsies from Becker muscular dystrophy (BMD), which does not involve denervation (Matsuo, 1996; Chevessier et al., 2004; Shelley and Colquhoun, 2005;

Mitchell and Borasio, 2007). Histologically, muscles from AD-EDMD patients showed morphological features of denervated muscle similar to ALS and CMS patients and distinct from BMD. As in ALS and CMS patients, AD-EDMD muscles were characterized by large variations in fiber diameter, numerous angular atrophic fibers, or round hypotrophic fibers as well as few centrally located nuclei, most nuclei being in a subsarcolemmal position (Fig. 7 B). In contrast, BMD muscles showed a majority of large centronucleated fibers typical of cycles of necrosis and regeneration (Fig. 7 B).

With regards to gene expression, similar to what was observed in AD-EDMD mouse models, all AD-EDMD patients showed gene expression profiles distinct from normal controls and were more similar to the denervation syndromes ALS and CMS (Fig. 7 C). *CHRNG*, *CHRNA*, *MYOG*, *MYOD1*, and *FBXO32* expression levels were all significantly elevated compared with normal volunteers (Fig. 7 C) and were often even higher than those in patients affected by the innervation-related diseases ALS and CMS. Importantly, expression levels of these genes were distinct from those of patients affected by BMD, which showed expression levels of these genes close or similar to normal volunteers (Fig. 7 C). The up-regulation of *MYOD1* in BMD is likely due to the activation of satellite cells and extensive muscle regeneration in this disease (Bhagavati et al., 1996). In contrast, *CHRNG*, *CHRNA*, *MYOG*, and *FBXO32* expression levels were low and similar to normal levels in patients with LGMD1B, a striated muscle laminopathy, and a patient affected by a FPLD with DCM-CD (FPLD-DCM-CD; van der Kooi et al., 2002), a laminopathy in which the fat tissue and heart muscle are affected (Fig. 7, A and C). This points to the fact that there is no innervation defect in these laminopathies and that denervation is not a general feature of muscular dystrophies or striated muscle laminopathies.

Consistent with functional denervation of muscle in AD-EDMD patients and our observations in AD-EDMD mouse models, nuclei from atrophic AD-EDMD muscle fibers also showed high levels of H3-K9 histone acetylation compared with normal controls (Fig. 7 B, asterisks). Importantly, increased histone acetylation was also observed in muscle fibers that did not show any physiological signs of atrophy, which suggests that the histone hyperacetylation is an early event preceding atrophy (Fig. 7 B, arrowheads). Similar patterns were also observed in muscles from ALS (not depicted) and CMS patients (Fig. 7 B) or using acetylated histone H4 antibody (not depicted). Collectively, these results support the presence of innervation defects in skeletal muscle from AD-EDMD patients.

Discussion

We have investigated here the molecular mechanisms by which mutations in the nuclear architectural proteins lamin A and C give rise to muscular dystrophy. We demonstrate that muscle in two established mouse models of EDMD exhibit altered innervation patterns and abnormal NMJ morphology. As a consequence, AD-EDMD mouse models show signs of innervation defects including misexpression of electrical activity–dependent genes and altered epigenetic chromatin modifications. The

same molecular defects occur in muscle from AD-EDMD patients with *LMNA* mutations. At the molecular level, we show that several nuclear envelope proteins involved in proper positioning of nuclei near the synapse are mislocalized in AD-EDMD mouse models, and recruitment of synaptic nuclei is impaired. These results provide insights into the cellular and molecular mechanisms for the muscle-specific phenotype of AD-EDMD, and they strongly suggest that NMJ defects contribute to the AD-EDMD disease phenotype.

NMJ defects in AD-EDMD

The molecular basis of how mutations in A-type lamins lead to muscle dystrophy has been elusive. One model is based on the observation that immortalized $Lmna^{-/-}$ myoblasts are impaired in their differentiation to myotubes (Frock et al., 2006); however, in vivo regeneration of cardiotoxin-treated $Lmna^{-/-}$ muscles is normal and primary $Lmna^{-/-}$ myoblast cultures do not show impairment in their differentiation to myotubes (Melcon et al., 2006).

We provide several lines of evidence for a model involving NMJ defects in AD-EDMD. First, innervation patterns and NMJ morphology are altered in two independent mouse models of AD-EDMD. Second, synaptic nuclei fail to be recruited to the NMJ in the animal models. Third, several electrical activity–dependent genes are misregulated, and denervation-characteristic histone modification patterns are present in AD-EDMD mouse model and patient samples, likely as a consequence of defective NMJ morphology. Furthermore, the proportion of altered NMJs in transient *Lmna* knockdown muscles strictly correlated with the number of histone hyperacetylated fibers, a hallmark of functional denervation. Fourth, our histological observations confirm previous reports (Mittelbronn et al., 2006) that muscles from AD-EDMD patients show morphological features similar to denervated muscles from ALS and CMS patients but were distinct from BMD. Finally, we found in mouse models and AD-EDMD patients that the gene expression pattern of several electrical activity–dependent genes resembles that of ALS, an established muscle denervation syndrome, and CMS, an established altered NMJ syndrome, but is distinct from the expression profile of these genes in BMD as well as two other *LMNA*-related diseases not associated with innervation defects.

Our findings of altered innervation and abnormal NMJ architecture in AD-EDMD muscle based on morphological and gene expression analysis are in line with observations on the electrical activity of AD-EDMD patient muscle. Conventional and single-fiber electromyography in a family with a variant of AD-EDMD caused by a *LMNA* mutation revealed electromyographic alterations in motor unit potentials that were suggestive of neurogenic muscular changes (Walter et al., 2005). Moreover, muscle biopsies of patients with AD-EDMD showed a mild mixed myopathic and neurogenic pattern with scattered small-angular atrophic myofibers, marked atrophy of type 1 fibers, and a clear predominance of type 2 fibers (Hong et al., 2005; Mittelbronn et al., 2006), which is similar to the slow-to-fast fiber switch observed in denervation (Stevens et al., 1999a,b). In addition, atrophied muscle fibers from AD-EDMD patients do not appear grouped, a hallmark of atrophy caused by degeneration

of the nerve cell (Rowinska-Marcinska et al., 2005). These physiological observations are consistent with the presence of the cellular and molecular defects observed in AD-EDMD mouse models and patient tissue reported here.

Our observations indicate that the abnormal innervation and NMJ defects are a cause and not a secondary consequence of altered, possibly chronic, muscle defects. This is supported by the fact that NMJ defects occur before any apparent muscle defects. We found altered innervation, failed synaptic nuclei recruitment, and SUN2 mislocalization in 6-wk-old *Lmna*$^{H222P/H222P}$ mice that are asymptomatic for muscle and locomotion defects (Arimura et al., 2005). In addition, all NMJ defects strongly correlate with the severity of symptoms in the animal models, and SUN2 aggregation occurred before NMJ alterations upon transient knockdown of A-type lamins. Although *Lmna*$^{-/-}$ animals exhibit axonal defects as previously reported (De Sandre-Giovannoli et al., 2002), the fact that transient knockdown of A-type lamins in muscle is sufficient to recapitulate the main phenotypes in the absence of nerve defects or muscle fibrosis indicates that loss of A-type lamins is causal for the NMJ phenotype. Because the AAV6 used here does not efficiently infect Schwann cells or the nerve, the NMJ defects must be caused by the impaired function of A-type lamins in the muscle and not the nerve. These results also suggest that the previously observed axonal defects in *Lmna*$^{-/-}$ mice are likely a consequence of loss of lamin function in muscle (De Sandre-Giovannoli et al., 2002). Based on these observations, we propose that the primary defect in muscular A-type lamin function leads to NMJ defects that ultimately contribute to the muscle atrophy observed in AD-EDMD.

A-type lamins mediate positioning of synaptic nuclei

Our data argue for a model in which A-type lamins play a structural role in organizing the molecular complexes responsible for the recruitment and positioning of synapse-associated nuclei underneath the postsynaptic membrane. In support, we show that the absence or mutation of A-type lamins causes mislocalization of two of the key components of the nuclear positioning machinery, the inner nuclear membrane protein SUN2 and the outer nuclear membrane component Nesprin-1, which links the nuclear envelope to the cytoskeleton. Strikingly, this mislocalization of SUN2 and Nesprin-1 was limited to synaptic nuclei but was not observed in extrasynaptic nuclei, which suggests a link between the organization of nuclear envelope components in synaptic nuclei and NMJ defects. We propose that as a consequence of this misorganization of the inner nuclear membrane, the number of muscle nuclei recruited at the synapse is reduced and the remaining synaptic nuclei beneath the NMJ tend to be progressively mislocalized or lost. This may lead to unstable NMJs, inefficient neurotransmission between the muscle and nerve, and innervation defects of the muscle fiber. Because the primary defect in both AD-EDMD mouse models is in the *Lmna* gene, these observations directly implicate A-type lamins and the SUN–Nesprin complex in the recruitment and positioning of synaptic nuclei. This interpretation is in line with earlier data demonstrating that Nesprin-1 and Nesprin-2 are mislocalized in

Lmna$^{-/-}$ fibroblasts (Libotte et al., 2005), that overexpression of a dominant-negative form of Nesprin-1 induces relocalization of synaptic nuclei at the periphery of the synapse (Grady et al., 2005), and that complete knockout of Nesprin-1 and Nesprin-2 in mice affects viability with immediate death at birth because of the complete absence of nuclei recruited to the synapses of diaphragm muscles (Zhang et al., 2007b).

It seems likely that A-type lamins act by organizing SUN proteins in the inner nuclear membrane, which then determines their interaction with Nesprins in the outer nuclear membrane (Hodzic et al., 2004; Padmakumar et al., 2005; Crisp et al., 2006; Haque et al., 2006). Interestingly, we find here differential effects of *Lmna* loss or *Lmna* mutations on SUN1 and SUN2. In synaptic nuclei, where SUN1 is expressed at low levels, SUN2 localization is dramatically affected by A-type lamins mutation or its absence; whereas, in extrasynaptic nuclei, where SUN1 is present, SUN2 localization is only slightly altered, suggesting that SUN1 might compensate for A-type lamins defects. Our findings point to the fact that, in muscle, SUN1 localization to the nuclear envelope is not dependent on A-type lamins, whereas SUN2 localization is, confirming biochemical studies showing that SUN1 and SUN2 localized to the nuclear envelope via different mechanisms (Padmakumar et al., 2005; Crisp et al., 2006; Haque et al., 2006; Wang et al., 2006). Our findings also confirm that SUN1 and SUN2 are not redundant and may play different roles in the inner nuclear membrane (Ding et al., 2007; Liu et al., 2007; Schmitt et al., 2007). Whether these interactions are primarily important for formation or maintenance of NMJs is not known.

Implications for candidate AD-EDMD genes

Our observations have implications for identification of additional AD-EDMD genes. Mutations in A-type lamins (*LMNA*) and emerin (*EMD*) currently only account for 50% of AD-EDMD patients (Zhang et al., 2007a). Our findings indicate that components involved in synaptic nuclei positioning are potential AD-EDMD candidate genes. This possibility has recently been validated by the identification of mutations in *SYNE1* and *SYNE2* in patients with AD-EDMD phenotypes (Zhang et al., 2007a). Moreover, Nesprin-1α and Nesprin-2β interactions with the nuclear envelope have been shown to be disrupted in X-linked EDMD cells, which suggests that emerin might also play a role in the synaptic nuclear envelope organization (Wheeler et al., 2007). Finally, Nesprin-2, emerin, LAP2α, and LAP2β localization has been shown to be disturbed in *LMNA* S143F progeria cells (Kandert et al., 2007), which suggests that the interaction between lamins and Nesprins may not only play a role in muscular laminopathies. In agreement with our data, so far no mutations in *SUN1* have been identified in AD-EDMD patients. Moreover, *SUN1*-deficient mice develop normally into adults without any evidence of muscular dystrophy (Ding et al., 2007), indicating that, at least in the presence of A-type lamins, SUN1 is dispensable during muscle development. However, here we show that the *SUN2* expression pattern is highly similar to *SYNE1* and that its localization is dramatically altered in AD-EDMD mouse model synaptic nuclei, which suggests it may be a crucial component of the synaptic nuclei envelope. For these

reasons, *SUN2* represents a novel gene candidate to be screened for mutation in AD-EDMD patients.

Tissue specificity of AD-EDMD

One of the most intriguing aspects of laminopathies is the question of how mutations in the ubiquitously expressed A-type lamin proteins lead to tissue-restricted disorders. We find here that various subsets of muscle nuclei express distinct combinations of the lamin-interacting proteins SUN1 and SUN2, and that this expression pattern correlates with susceptibility to AD-EDMD mutations. It is therefore possible that the tissue-specific nature of *LMNA* mutations is caused by the presence of particular combinations of lamin-interacting proteins in various tissues (Ellis, 2006). We find that AD-EDMD mutations in mice primarily affect the synaptic nuclei in the context of the pluri-nucleated muscle. Interestingly, synaptic nuclei only express SUN2 and Nesprin-1, whereas extrasynaptic nuclei express SUN1, SUN2, and Nesprin-1. Strikingly, Nesprin-1 and SUN2 are preferentially expressed at high levels in skeletal muscle and heart, both tissues affected in AD-EDMD (Apel et al., 2000; Sun et al., 2002). Moreover, SUN2 has been identified as one of the genes differentially expressed in congenital heart defects (Sun et al., 2002), which suggests that SUN2, and maybe Nesprin-1, alteration might affect heart physiology. Obviously, the cardiac defects in EDMD patients are not mediated through NMJ defects because cardiac muscle lacks NMJ. A possibility is that mutations in lamin A not only affect the nuclear envelope but also, via the SUN–Nesprin axis, the cytoskeleton, and possibly even the plasma membrane, as indicated by our finding of altered AChR organization at the cell surface. Interestingly, the ERK1/2–MAP kinase pathways whose upstream receptors are at the plasma membrane have recently been shown to be up-regulated in heart from $Lmna^{H222P/H222P}$ mice (Mejat et al., 2003; Muchir et al., 2007).

Collectively, our data suggest a mechanistic model for the laminopathy AD-EDMD. We propose that AD-EDMD mutations alter the structural organization of the nuclear envelope in synaptic nuclei of muscle fibers. As a result, the SUN–Nesprin-mediated interaction of the nucleus with the cytoskeleton is interrupted, leading to failed recruitment and mispositioning of synapse-associated myonuclei. Lamin A/C–mediated neurotransmission defects may result in the misregulation of electrical activity–dependent genes and to global chromatin rearrangements. These results strongly indicate that NMJ defects contribute to human AD-EDMD, and they provide insights into the cellular and molecular disease mechanism of a laminopathy.

Materials and methods

Animals
Lmna mice (*Lmna*$^{+/+}$, *Lmna*$^{+/-}$, and *Lmna*$^{-/-}$) and *Lmna*$^{H222P/H222P}$ (Arimura et al., 2005; Sullivan et al., 1999) were housed individually and provided with mouse chow and water ad libitum in restricted-access, specific-pathogen-free animal care facilities at the National Institutes of Health (Bethesda, MD) and the Institute of Myology (Paris, France), respectively. To avoid any influence from the genetic background, mutant mice were always compared with their wild-type littermates. All experimental procedures were performed on C57BL/6 male mice according to National Institutes of Health Animal Care Protocol approved by the National Cancer Institute Center for Cancer Research Animal Care and Use Committee.

Human samples
Patient muscle biopsies were obtained from diagnosis procedures either from Groupe Hospitalier Pitié-Salpêtrière Hospital (Paris, France) or from Children's National Medical Center (Washington DC) according to local ethical committee regulations. All biopsies were flash-frozen in isopentane cooled in liquid nitrogen immediately after excision and were stored in airtight hydrated containers until use. All muscle samples were tested histologically by cryosection and showed excellent preservation of muscle morphology by hematoxylin-eosin histology. Characteristics of the patient population are provided in Table S1.

Antibodies and immunostaining
Anti-LAP2, –Nesprin-1, -SUN1 and -SUN2 antibodies were gifts from K. Wilson (Johns Hopkins University School of Medicine, Baltimore, MD; Fischer et al., 2001), J. Sanes (Harvard University, Cambridge, MA; Grady et al., 2005), S. Shackleton (University of Leicester, Leicester, England, UK; Haque et al., 2006), and D. Hodzic (Washington University, St. Louis, MO; Hodzic et al., 2004; Crisp et al., 2006), respectively. As described in Grady et al. (2005), the antibody against Nesprin-1 (Syne-1) recognizes a region that is highly conserved in Nesprin-2 (Syne-2) and could therefore recognize both proteins. The lamin B antibody (Santa Cruz Biotechnology, Inc.) recognized lamin B1 and, to a lesser extent, lamin B2 and B3. Histone acetylation levels were evaluated using acetyl-histone H3-K9 and acetyl-histone H4 antibodies (Millipore). The NMJs were stained using the Alexa Fluor 488 conjugate Bgt (Invitrogen). Muscle fibers were delineated on tissue section using α2-laminin antibody, clone 4H8-2 (Sigma-Aldrich), a component of the extracellular lamina.

Immunofluorescence experiments and Bgt staining on diaphragms and isolated muscle fibers were performed as described previously (Koenen et al., 2005; Mejat et al., 2005).

Diaphragms were flat-mounted in Vectashield mounting medium containing DAPI (H-1200; Vector Laboratories). Z serial images were collected using a UPlanApo 10× 0.40 objective lens (Olympus) on a microscope (DeltaVision IX70; Olympus) controlled by a Deltavision system (Applied Precision, LLC) and fitted with a charge-coupled device camera (CoolSnap; Photometrics). Image stacks were deconvolved using SoftWoRx 3.5.1 (Applied Precision, LLC) and projected into a single image. Because of the size of the diaphragm, multiple z serial images were taken to cover the whole diaphragm, then the projected images were combined using SoftWoRx 3.5.1 or Photoshop CS3 (Adobe). When necessary, brightness and contrast adjustments were applied to the whole reconstituted image using Photoshop CS3. The width of the innervation area was defined as the distance between the two AChR clusters located at the maximal distance from the main axis of the diaphragm. For each diaphragm, a minimum of 200 measurements regularly spaced along the length of the diaphragm were taken. At least three diaphragms of each genotype (wild type, $Lmna^{H222P/H222P}$, and $Lmna^{-/-}$) were quantified using ImageJ (National Institutes of Health).

For immunofluorescence microscopy on mouse muscle fibers, tibialis anterior muscles were dissected and fixed in 4% PFA/PBS for 30 min at RT, rinsed with PBS, pH 7.5, at RT, and permeabilized and blocked in the blocking buffer (1% BSA/0.5% Triton X-100/PBS) overnight at 4°C. They were then incubated overnight at 4°C with the primary antibody (1:500) in blocking buffer. Samples were washed three times for 1 h each time in 0.5% Triton X-100/PBS, incubated with secondary antibody (Alexa Fluor 568 goat anti–rabbit, 1:500; Invitrogen) and Bgt–Alexa Fluor conjugate (1:1,000) for 1 h at RT in blocking buffer, and then washed three times for 1 h each time in 0.5% Triton X-100/PBS, plus an overnight incubation at 4°C. Finally, isolated muscle fibers were flat-mounted in mounting medium containing DAPI. Z serial images were collected using a PlanApo 100× 1.4 lens (Nikon) on an Eclipse E800 (Nikon), and image stacks were projected into a single image using Metamorph 6.3 software (MDS Analytical Technologies). A minimum of 100 fibers from at least three different mice of each genotype were analyzed for each staining.

For immunofluorescence microscopy on human muscle biopsies, tissue sections were fixed in 4% PFA/PBS for 10 min at RT, rinsed with PBS, pH 7.5, at RT, permeabilized in 1% Triton X-100/PBS for 30 min at RT, and then blocked in 2% BSA in PBS for 30 min at RT. After an overnight incubation at 4°C with the primary anti-acetylated histone and anti–α2-laminin antibodies (1:200) in blocking buffer, the samples were washed three times in 0.5% Triton X-100 in PBS, incubated with secondary antibodies (Alexa Fluor 488 donkey anti–Rat IgG and Alexa Fluor 568 goat anti–rabbit, 1:500; Invitrogen) for 1 h at RT in blocking buffer, and then washed three times in PBS. Finally, tissue sections were flat-mounted in DAPI-containing mounting media.

Z serial images were collected using a PlanApo 20× 0.75 NA lens (Nikon) on an Eclipse E800, and image stacks were projected into a single image using Metamorph 6.3 software. For all imaging, exposure settings were identical between compared samples and genotypes.

Counting of synaptic and perisynaptic nuclei
Quantification of synaptic and perisynaptic nuclei was performed as described previously (Grady et al., 2005). In brief, a nucleus was defined as synaptic when at least 25% of the DAPI and Nesprin-1 or SUN2 signal overlapped with the Bgt-positive site, and a perisynaptic nucleus was defined as one for which the DAPI and Nesprin-1 signal did not overlap with the Bgt-positive site but was less than half its diameter from the edge of a site. A minimum of 100 NMJs from at least three different mice of each genotype were analyzed.

Real-time quantitative RT-PCR
Gene expression was evaluated by quantitative RT-PCR (MyiQ; Bio-Rad Laboratories) using the iQ SYBR Green Supermix (Bio-Rad Laboratories) on total RNA extracted (RNA fibrous tissue mini kit; QIAGEN) from homogenized (in RLT buffer; TissueRuptor Homogenizer; QIAGEN) whole mouse gastrocnemius muscles or human tissue sections. 500 µg of total RNA was reverse-transcribed using Superscript III (Invitrogen) according to manufacturer's instructions. All measures were normalized to *GAPDH* RNA levels. The sequences of the mouse primers are provided in Table S2. For each mouse, the two gastrocnemius muscles were analyzed separately, providing two measures per mouse, and the gene expression levels were evaluated in at least three mice per phenotype (wild type, *Lmna*$^{H222P/H222P}$, and *Lmna*$^{-/-}$). Mice of a given age were compared with their wild-type littermates. The sequences of the mouse and human primers are provided in Table S2.

AAV vector construction, viral production, and in vivo administration
The AAV vector containing the GFP reporter gene (dsAAV-cytomegalovirus [CMV]-GFP) has been described previously (Wang et al., 2003). As a preliminary experiment, 50 µl (1 × 10^{12} viral particles/ml) of AAV2-GFP, AAV6-GFP, AAV7-GFP, or AAV8-GFP was directly injected into the tibialis anterior of 6-wk-old male C57BL/6 mice using a U-100 insulin syringe. Muscles fibers were assessed for GFP expression by fluorescent microscopy 1 wk after injection. At least three muscles per AAV serotype were analyzed. AAV6 was used in future experiments because this serotype showed a high transduction efficiency of muscle fibers (> 90%) and no nonmuscle cell transduction.

AAV6 vectors containing the shRNA gene against EGFP or LMNA were made by cloning the short hairpin oligonucleotides into the plasmid pSilencer-1.0-U6 (Applied Biosystems) using ApaI and EcoRI sites. The U6-shRNA expression cassettes were then subcloned into a dsAAV-CMV-GFP vector by replacing the CMV promoter using KpnI and EagI sites. The 19-mer shRNA target sequence for EGFP was 5′-CGGCCACAAGTTCAGCGTG-3′ and the sequence for LMNA was 5′-GGAGCTTGACTTCCAGAAG-3′. Recombinant AAV6 vectors were produced as described previously (Wang et al., 2005). For intramuscular injection, 50 µl (1 × 10^{12} viral particles/ml) of viral solution was directly injected into the left tibialis anterior of 6-wk-old male C57BL/6 mice using a U-100 insulin syringe. 1–5 wk after injection, for each time point, a minimum of six mice were killed, and their injected muscles were assessed by quantitative RT-PCR, Western blotting, or immunofluorescence. For each mouse, the right contralateral noninjected tibialis anterior was used as control (noninjected).

Western blot
Frozen tibialis anterior muscles were homogenized in a total protein extraction buffer (2% SDS, 250 mM sucrose, 75 mM urea, 1 mM dithiothreitol, and 50 mM Tris-HCl, pH 7.5) with protease inhibitor (protease inhibitor cocktail III; EMD) by TissueRuptor System (QIAGEN). After determination of protein concentration, equal amounts of total proteins were separated on 7.5% SDS-PAGE gels and hybridized with primary goat lamin A/C antibody (1:1,000; Santa Cruz Biotechnology, Inc.) or primary mouse histone H3 antibody (1:1,000; Abcam) and with secondary donkey anti–goat (1:1,000; Santa Cruz Biotechnology, Inc.) or rabbit anti–mouse IgG HRP-conjugated antibodies (Amersham enhanced chemiluminescence [ECL] Western blot analysis system; GE Healthcare). Recognized proteins were visualized with an ECL Western blot analysis system (GE Healthcare).

Statistical analysis
Statistical analysis was performed with the unpaired, unequal variances, two-tailed Student's *t* test using Excel software (Microsoft).

Online supplemental material
Fig. S1 presents SUN1, SUN2, and Nesprin-1 localizations in muscle fibers in wild-type and mutant mice. Fig. S2 shows synaptic nuclei acetylation levels in wild-type and mutant *Lmna* mice. Fig. S3 presents GFP expression in muscle fibers and transient knockdown of *LMNA* using AAV. Table S1 describes the patients and normal volunteers included in this study. Table S2 presents the sequences of the primers used in quantitative PCR experiments. Online supplemental material is available at http://www.jcb.org/cgi/content/full/jcb.200811035/DC1.

References

Apel, E.D., R.M. Lewis, R.M. Grady, and J.R. Sanes. 2000. Syne-1, a dystrophin- and Klarsicht-related protein associated with synaptic nuclei at the neuromuscular junction. *J. Biol. Chem.* 275:31986–31995.

Arimura, T., A. Helbling-Leclerc, C. Massart, S. Varnous, F. Niel, E. Lacene, Y. Fromes, M. Toussaint, A.M. Mura, D.I. Keller, et al. 2005. Mouse model carrying H222P-Lmna mutation develops muscular dystrophy and dilated cardiomyopathy similar to human striated muscle laminopathies. *Hum. Mol. Genet.* 14:155–169.

Bakay, M., Z. Wang, G. Melcon, L. Schiltz, J. Xuan, P. Zhao, V. Sartorelli, J. Seo, E. Pegoraro, C. Angelini, et al. 2006. Nuclear envelope dystrophies show a transcriptional fingerprint suggesting disruption of Rb-MyoD pathways in muscle regeneration. *Brain.* 129:996–1013.

Bhagavati, S., A. Ghatpande, S.A. Shafiq, and B. Leung. 1996. In situ hybridization analysis for expression of myogenic regulatory factors in regenerating muscle of mdx mouse. *J. Neuropathol. Exp. Neurol.* 55:509–514.

Broers, J.L., E.A. Peeters, H.J. Kuijpers, J. Endert, C.V. Bouten, C.W. Oomens, F.P. Baaijens, and F.C. Ramaekers. 2004. Decreased mechanical stiffness in LMNA−/− cells is caused by defective nucleo-cytoskeletal integrity: implications for the development of laminopathies. *Hum. Mol. Genet.* 13:2567–2580.

Broers, J.L., F.C. Ramaekers, G. Bonne, R.B. Yaou, and C.J. Hutchison. 2006. Nuclear lamins: laminopathies and their role in premature ageing. *Physiol. Rev.* 86:967–1008.

Burke, B., and C.L. Stewart. 2002. Life at the edge: the nuclear envelope and human disease. *Nat. Rev. Mol. Cell Biol.* 3:575–585.

Burke, B., and C.L. Stewart. 2006. The laminopathies: the functional architecture of the nucleus and its contribution to disease. *Annu. Rev. Genomics Hum. Genet.* 7:369–405.

Chevessier, F., B. Faraut, A. Ravel-Chapuis, P. Richard, K. Gaudon, S. Bauche, C. Prioleau, R. Herbst, E. Goillot, C. Ioos, et al. 2004. MUSK, a new target for mutations causing congenital myasthenic syndrome. *Hum. Mol. Genet.* 13:3229–3240.

Crisp, M., Q. Liu, K. Roux, J.B. Rattner, C. Shanahan, B. Burke, P.D. Stahl, and D. Hodzic. 2006. Coupling of the nucleus and cytoplasm: role of the LINC complex. *J. Cell Biol.* 172:41–53.

De Sandre-Giovannoli, A., M. Chaouch, S. Kozlov, J.M. Vallat, M. Tazir, N. Kassouri, P. Szepetowski, T. Hammadouche, A. Vandenberghe, C.L. Stewart, et al. 2002. Homozygous defects in LMNA, encoding lamin A/C nuclear-envelope proteins, cause autosomal recessive axonal neuropathy in human (Charcot-Marie-Tooth disorder type 2) and mouse. *Am. J. Hum. Genet.* 70:726–736.

Ding, X., R. Xu, J. Yu, T. Xu, Y. Zhuang, and M. Han. 2007. SUN1 is required for telomere attachment to nuclear envelope and gametogenesis in mice. *Dev. Cell.* 12:863–872.

Duclert, A., J. Piette, and J.P. Changeux. 1991. Influence of innervation of myogenic factors and acetylcholine receptor alpha-subunit mRNAs. *Neuroreport.* 2:25–28.

Ellis, J.A. 2006. Emery-Dreifuss muscular dystrophy at the nuclear envelope: 10 years on. *Cell. Mol. Life Sci.* 63:2702–2709.

Fischer, A.H., P. Taysavang, C.J. Weber, and K.L. Wilson. 2001. Nuclear envelope organization in papillary thyroid carcinoma. *Histol. Histopathol.* 16:1–14.

Frock, R.L., B.A. Kudlow, A.M. Evans, S.A. Jameson, S.D. Hauschka, and B.K. Kennedy. 2006. Lamin A/C and emerin are critical for skeletal muscle satellite cell differentiation. *Genes Dev.* 20:486–500.

Gomes, M.D., S.H. Lecker, R.T. Jagoe, A. Navon, and A.L. Goldberg. 2001. Atrogin-1, a muscle-specific F-box protein highly expressed during muscle atrophy. *Proc. Natl. Acad. Sci. USA.* 98:14440–14445.

Grady, R.M., D.A. Starr, G.L. Ackerman, J.R. Sanes, and M. Han. 2005. Syne proteins anchor muscle nuclei at the neuromuscular junction. *Proc. Natl. Acad. Sci. USA.* 102:4359–4364.

Haque, F., D.J. Lloyd, D.T. Smallwood, C.L. Dent, C.M. Shanahan, A.M. Fry, R.C. Trembath, and S. Shackleton. 2006. SUN1 interacts with nuclear lamin A and cytoplasmic nesprins to provide a physical connection between the nuclear lamina and the cytoskeleton. *Mol. Cell. Biol.* 26:3738–3751.

Hodzic, D.M., D.B. Yeater, L. Bengtsson, H. Otto, and P.D. Stahl. 2004. Sun2 is a novel mammalian inner nuclear membrane protein. *J. Biol. Chem.* 279:25805–25812.

Hong, J.S., C.S. Ki, J.W. Kim, Y.L. Suh, J.S. Kim, K.K. Baek, B.J. Kim, K.J. Ahn, and D.K. Kim. 2005. Cardiac dysrhythmias,cardiomyopathy and muscular dystrophy in patients with Emery-Dreifuss muscular dystrophy and limb-girdle muscular dystrophy type 1B. *J. Korean Med. Sci.* 20:283–290.

Kandert, S., Y. Luke, T. Kleinhenz, S. Neumann, W. Lu, V.M. Jaeger, M. Munck, M. Wehnert, C.R. Muller, Z. Zhou, et al. 2007. Nesprin-2 giant safeguards nuclear envelope architecture in LMNA S143F progeria cells. *Hum. Mol. Genet.* 16:2944–2959.

Koenen, M., C. Peter, A. Villarroel, V. Witzemann, and B. Sakmann. 2005. Acetylcholine receptor channel subtype directs the innervation pattern of skeletal muscle. *EMBO Rep.* 6:570–576.

Libotte, T., H. Zaim, S. Abraham, V.C. Padmakumar, M. Schneider, W. Lu, M. Munck, C. Hutchison, M. Wehnert, B. Fahrenkrog, et al. 2005. Lamin A/C-dependent localization of Nesprin-2, a giant scaffolder at the nuclear envelope. *Mol. Biol. Cell.* 16:3411–3424.

Liu, Q., N. Pante, T. Misteli, M. Elsagga, M. Crisp, D. Hodzic, B. Burke, and K.J. Roux. 2007. Functional association of Sun1 with nuclear pore complexes. *J. Cell Biol.* 178:785–798.

Matsuo, M. 1996. Duchenne/Becker muscular dystrophy: from molecular diagnosis to gene therapy. *Brain Dev.* 18:167–172.

Mattout, A., T. Dechat, S.A. Adam, R.D. Goldman, and Y. Gruenbaum. 2006. Nuclear lamins, diseases and aging. *Curr. Opin. Cell Biol.* 18:335–341.

Mejat, A., A. Ravel-Chapuis, M. Vandromme, and L. Schaeffer. 2003. Synapse-specific gene expression at the neuromuscular junction. *Ann. N. Y. Acad. Sci.* 998:53–65.

Mejat, A., F. Ramond, R. Bassel-Duby, S. Khochbin, E.N. Olson, and L. Schaeffer. 2005. Histone deacetylase 9 couples neuronal activity to muscle chromatin acetylation and gene expression. *Nat. Neurosci.* 8:313–321.

Melcon, G., S. Kozlov, D.A. Cutler, T. Sullivan, L. Hernandez, P. Zhao, S. Mitchell, G. Nader, M. Bakay, J.N. Rottman, et al. 2006. Loss of emerin at the nuclear envelope disrupts the Rb1/E2F and MyoD pathways during muscle regeneration. *Hum. Mol. Genet.* 15:637–651.

Merlie, J.P., J. Mudd, T.C. Cheng, and E.N. Olson. 1994. Myogenin and acetylcholine receptor alpha gene promoters mediate transcriptional regulation in response to motor innervation. *J. Biol. Chem.* 269:2461–2467.

Mitchell, J.D., and G.D. Borasio. 2007. Amyotrophic lateral sclerosis. *Lancet.* 369:2031–2041.

Mittelbronn, M., F. Hanisch, M. Gleichmann, M. Stotter, R. Korinthenberg, M. Wehnert, G. Bonne, S. Rudnik-Schoneborn, and A. Bornemann. 2006. Myofiber degeneration in autosomal dominant Emery-Dreifuss muscular dystrophy (AD-EDMD) (LGMD1B). *Brain Pathol.* 16:266–272.

Mounkes, L., S. Kozlov, B. Burke, and C.L. Stewart. 2003. The laminopathies: nuclear structure meets disease. *Curr. Opin. Genet. Dev.* 13:223–230.

Muchir, A., P. Pavlidis, V. Decostre, A.J. Herron, T. Arimura, G. Bonne, and H.J. Worman. 2007. Activation of MAPK pathways links LMNA mutations to cardiomyopathy in Emery-Dreifuss muscular dystrophy. *J. Clin. Invest.* 117:1282–1293.

Padmakumar, V.C., T. Libotte, W. Lu, H. Zaim, S. Abraham, A.A. Noegel, J. Gotzmann, R. Foisner, and I. Karakesisoglou. 2005. The inner nuclear membrane protein Sun1 mediates the anchorage of Nesprin-2 to the nuclear envelope. *J. Cell Sci.* 118:3419–3430.

Ravel-Chapuis, A., M. Vandromme, J.L. Thomas, and L. Schaeffer. 2007. Postsynaptic chromatin is under neural control at the neuromuscular junction. *EMBO J.* 26:1117–1128.

Rowinska-Marcinska, K., E. Szmidt-Salkowska, A. Fidzianska, E. Zalewska, M. Dorobek, A. Karwanska, and I. Hausmanowa-Petrusewicz. 2005. Atypical motor unit potentials in Emery-Dreifuss muscular dystrophy (EDMD). *Clin. Neurophysiol.* 116:2520–2527.

Ruegg, M.A. 2005. Organization of synaptic myonuclei by Syne proteins and their role during the formation of the nerve-muscle synapse. *Proc. Natl. Acad. Sci. USA.* 102:5643–5644.

Sandri, M., C. Sandri, A. Gilbert, C. Skurk, E. Calabria, A. Picard, K. Walsh, S. Schiaffino, S.H. Lecker, and A.L. Goldberg. 2004. Foxo transcription factors induce the atrophy-related ubiquitin ligase atrogin-1 and cause skeletal muscle atrophy. *Cell.* 117:399–412.

Schaeffer, L., A. de Kerchove d'Exaerde, and J.P. Changeux. 2001. Targeting transcription to the neuromuscular synapse. *Neuron.* 31:15–22.

Schmitt, J., R. Benavente, D. Hodzic, C. Hoog, C.L. Stewart, and M. Alsheimer. 2007. Transmembrane protein Sun2 is involved in tethering mammalian meiotic telomeres to the nuclear envelope. *Proc. Natl. Acad. Sci. USA.* 104: 7426–7431.

Shelley, C., and D. Colquhoun. 2005. A human congenital myasthenia-causing mutation (epsilon L78P) of the muscle nicotinic acetylcholine receptor with unusual single channel properties. *J. Physiol.* 564:377–396.

Starr, D.A., and M. Han. 2002. Role of ANC-1 in tethering nuclei to the actin cytoskeleton. *Science.* 298:406–409.

Stevens, L., B. Gohlsch, Y. Mounier, and D. Pette. 1999a. Changes in myosin heavy chain mRNA and protein isoforms in single fibers of unloaded rat soleus muscle. *FEBS Lett.* 463:15–18.

Stevens, L., K.R. Sultan, H. Peuker, B. Gohlsch, Y. Mounier, and D. Pette. 1999b. Time-dependent changes in myosin heavy chain mRNA and protein isoforms in unloaded soleus muscle of rat. *Am. J. Physiol.* 277:C1044–C1049.

Sullivan, T., D. Escalante-Alcalde, H. Bhatt, M. Anver, N. Bhat, K. Nagashima, C.L. Stewart, and B. Burke. 1999. Loss of A-type lamin expression compromises nuclear envelope integrity leading to muscular dystrophy. *J. Cell Biol.* 147:913–920.

Sun, G., S. Yuen Chan, Y. Yuan, K. Wang Chan, G. Qiu, K. Sun, and M. Ping Leung. 2002. Isolation of differentially expressed genes in human heart tissues. *Biochim. Biophys. Acta.* 1588:241–246.

van der Kooi, A.J., G. Bonne, B. Eymard, D. Duboc, B. Talim, M. Van der Valk, P. Reiss, P. Richard, L. Demay, L. Merlini, et al. 2002. Lamin A/C mutations with lipodystrophy, cardiac abnormalities, and muscular dystrophy. *Neurology.* 59:620–623.

Walter, M.C., T.N. Witt, B.S. Weigel, P. Reilich, P. Richard, D. Pongratz, G. Bonne, M.S. Wehnert, and H. Lochmuller. 2005. Deletion of the LMNA initiator codon leading to a neurogenic variant of autosomal dominant Emery-Dreifuss muscular dystrophy. *Neuromuscul. Disord.* 15:40–44.

Wang, Q., X. Du, Z. Cai, and M.I. Greene. 2006. Characterization of the structures involved in localization of the SUN proteins to the nuclear envelope and the centrosome. *DNA Cell Biol.* 25:554–562.

Wang, Z., H.I. Ma, J. Li, L. Sun, J. Zhang, and X. Xiao. 2003. Rapid and highly efficient transduction by double-stranded adeno-associated virus vectors in vitro and in vivo. *Gene Ther.* 10:2105–2111.

Wang, Z., T. Zhu, C. Qiao, L. Zhou, B. Wang, J. Zhang, C. Chen, J. Li, and X. Xiao. 2005. Adeno-associated virus serotype 8 efficiently delivers genes to muscle and heart. *Nat. Biotechnol.* 23:321–328.

Wheeler, M.A., J.D. Davies, Q. Zhang, L.J. Emerson, J. Hunt, C.M. Shanahan, and J.A. Ellis. 2007. Distinct functional domains in nesprin-1alpha and nesprin-2beta bind directly to emerin and both interactions are disrupted in X-linked Emery-Dreifuss muscular dystrophy. *Exp. Cell Res.* 313:2845–2857.

Wilson, K.L. 2000. The nuclear envelope, muscular dystrophy and gene expression. *Trends Cell Biol.* 10:125–129.

Worman, H.J., and G.G. Gundersen. 2006. Here come the SUNs: a nucleocytoskeletal missing link. *Trends Cell Biol.* 16:67–69.

Worman, H.J., and G. Bonne. 2007. "Laminopathies": a wide spectrum of human diseases. *Exp. Cell Res.* 313:2121–2133.

Zhang, Q., J.N. Skepper, F. Yang, J.D. Davies, L. Hegyi, R.G. Roberts, P.L. Weissberg, J.A. Ellis, and C.M. Shanahan. 2001. Nesprins: a novel family of spectrin-repeat-containing proteins that localize to the nuclear membrane in multiple tissues. *J. Cell Sci.* 114:4485–4498.

Zhang, Q., C. Bethmann, N.F. Worth, J.D. Davies, C. Wasner, A. Feuer, C.D. Ragnauth, Q. Yi, J.A. Mellad, D.T. Warren, et al. 2007a. Nesprin-1 and -2 are involved in the pathogenesis of Emery Dreifuss muscular dystrophy and are critical for nuclear envelope integrity. *Hum. Mol. Genet.* 16:2816–2833.

Zhang, X., R. Xu, B. Zhu, X. Yang, X. Ding, S. Duan, T. Xu, Y. Zhuang, and M. Han. 2007b. Syne-1 and Syne-2 play crucial roles in myonuclear anchorage and motor neuron innervation. *Development.* 134:901–908.